Electromagnetically induced absorption scheme for vapor-cell atomic clock

DENIS BRAZHNIKOV,[1,2,3] STEPAN IGNATOVICH,[1] VLADISLAV VISHNYAKOV,[1] RODOLPHE BOUDOT,[4,5] AND MIKHAIL SKVORTSOV[1]

[1] *Institute of Laser Physics SB RAS, 15B Lavrentyev ave., Novosibirsk 630090, Russia*
[2] *Novosibirsk State University, 2 Pirogov str., Novosibirsk 630090, Russia*
[3] *brazhnikov@laser.nsc.ru*
[4] *FEMTO-ST, CNRS, UBFC, ENSMM, 26 rue de l'épitaphe, Besançon 25000, France*
[5] *rodolphe.boudot@femto-st.fr*

Abstract: A dual-frequency light field scheme, composed of counterpropagating pump and probe light waves with equal circular polarizations and different intensities, is proposed for the detection of subnatural-linewidth electromagnetically induced absorption (EIA) resonances. In this scheme, the bright-type EIA resonance is obtained at fixed static magnetic field by tuning the frequency difference between both optical fields and can be used as a frequency reference in an atomic clock. Using a 5-mm long buffer-gas-filled Cs vapor cell, an EIA-based atomic clock with a short-term fractional frequency stability of $5.8 \times 10^{-12}\ \tau^{-1/2}$ until 20 s integration time is reported. These performances are found to be in correct agreement with the signal-to-noise/linewidth ratio of the resonance. The proposed EIA scheme can be considered as an alternative approach to the coherent population trapping (CPT) technique for the development of compact atomic clocks and sensors.

1. Introduction

Quantum coherent superposition of atomic states created by the simultaneous interaction of two coherent light fields are extensively used in nonlinear spectroscopy [1] and find many exciting applications in quantum sensing, quantum information, laser cooling [2] and atomic devices [3]. These phenomena, including mainly electromagnetically induced transparency (EIT) [4], coherent population trapping (CPT) [5, 6], electromagnetically induced absorption (EIA) [7] and other atomic three-level configurations [8], imply the creation of a specific non-absorbing (non-transmitting) quantum "dark" ("bright") state that yields the detection of narrow subnatural-linewidth dark (bright) resonances in the absorption profiles.

Among these different approaches, the coherent population trapping phenomenon has known a great success for the development of atomic clocks. In CPT physics [5], atoms are driven by the combined action of two resonant optical fields into a non-interacting dark state uncoupled from the excited state when the null Raman detuning condition is satisfied. The microwave CPT resonance linewidth is limited by the relaxation rate of the atomic ground state coherence and can be reduced with buffer-gas-filled cells [9, 10], wall-coated cells [11–13], or through the use of cold atom samples [14]. The CPT resonance contrast, defined as the ratio between the resonance signal amplitude and the dc background level, depends strongly on the light-field polarization scheme.

In most compact CPT clocks, atoms interact with a circularly polarized field (σ–σ configuration) [15]. However, this scheme tends to accumulate many atoms into extreme Zeeman sub-levels and yields the detection of low-contrast CPT resonances onto the magnetic-field insensitive "0-0" clock transition. To circumvent this issue, different optimized CPT pumping schemes, generally based on the alkali D_1 line [16], have been proposed [17–24]. Such polarization schemes, combined with pulsed Ramsey-like interrogation protocols [21, 25], have led to the

demonstration of high-stability CPT atomic clocks [26–29].

At the contrary of the CPT or EIT [30] approaches involving the detection of dark resonances, the exploitation of coherently driven bright resonances has been rarely explored for the development of atomic clocks. In [31], a bright three-photon N-type resonance has been used on the Rb D_1 line for the demonstration of an atomic clock. The electromagnetically induced absorption (EIA) two-photon resonance, discovered in [7] and explained initially as the result of a spontaneous transfer of Zeeman coherences or magnetic sub-level populations from the excited state to the ground state [32–34], is an alternative option for the detection of narrow "bright" resonances.

A relevant number of EIA-based schemes and experiments using single-frequency magneto-optical (Hanle-like) configurations or dual-frequency light-field configurations have been reported in the literature [35–54]. It should be noted that in many of these works, the physical origin of the EIA effect differs from the process of spontaneous transfer of Zeeman coherences or populations identified in pioneering EIA studies [7, 36]. In any case, none of the previously proposed EIA schemes was suitable for atomic clock operation since the high-quality EIA resonance was observed in the magneto-optical configuration (mostly single-frequency Hanle-like resonances). To demonstrate an EIA-based atomic clock, the EIA scheme should involve a light field composed of at least two optical frequencies ν_1 and ν_2 separated by the microwave frequency $\nu_\mu = \nu_1 - \nu_2$. To the best of our knowledge, such an EIA-scheme compliant with the development of an EIA-based clock has never been proposed.

In this article, we report a novel excitation scheme for the detection of subnatural-linewidth EIA resonances on the cesium D_1 line, adapted for atomic clock operation. A buffer-gas-filled vapor cell is irradiated by dual-frequency counterpropagating control (pump) and probe beams with equal circular polarizations and different intensities. The bright-type EIA resonance is detected by tuning the laser frequency difference between both optical fields, at fixed static magnetic field. The proposed scheme is applied for the demonstration of an all-optical EIA-based atomic clock using a 5-mm long cell. The latter demonstrates a preliminary short-term fractional frequency stability of $5.8 \times 10^{-12}\ \tau^{-1/2}$ until 20 s integration time, found to be in correct agreement with the signal-to-noise/linewidth limit. This EIA scheme might be viewed as an alternative to CPT for the development of compact atomic clocks and quantum sensors.

2. EIA scheme

2.1. Experimental setup

Figure 1(a) depicts the experimental setup used for EIA resonance spectroscopy and clock. The laser field is produced by a distributed-Bragg resonator (DBR) laser tuned on the Cs D_1 line (λ=894.6 nm), with a spectral linewidth narrower than 1 MHz. A fiber-coupled intensity Mach-Zehnder electro-optic modulator (EOM, iXblue NIR-MX950-LN-20) driven by a microwave frequency synthesizer is used to produce an optical field composed of two resonant angular optical frequencies ω_1 and ω_2 separated by $\Delta_g \approx 2\pi \times 9.192$ GHz. At the output of the EOM, a neutral-density filter (NF) controls the total light power sent into the cell. A polarizing beam splitter PBS1 serves as a polarizer. The combination of PBS1 and PBS2 allows to separate the laser beam into a probe beam and a control beam, propagating ultimately into the Cs vapor cell in opposite directions with equal circular polarizations (obtained thanks to quarter-wave plates QWP1 and QWP2) and different intensities. The PBS2 is also used to send the probe beam at the output of the cell into the photodiode PD. The PBS3 is used to filter the backward control beam. The Gaussian diameter of the control beam is about 5 mm. The probe beam diameter is controlled by an iris diaphragm and equals 5 mm.

The output signal from the photodiode is used both for the stabilization of the microwave synthesizer local oscillator (LO) frequency onto the EIA resonance, and for the stabilization of the laser frequency onto the Doppler absorption profile. The cell is a borosilicate glass-blown Cs vapor cell with length 5 mm and diameter 25 mm. The cell is filled with Ne-Ar buffer-gas mixture

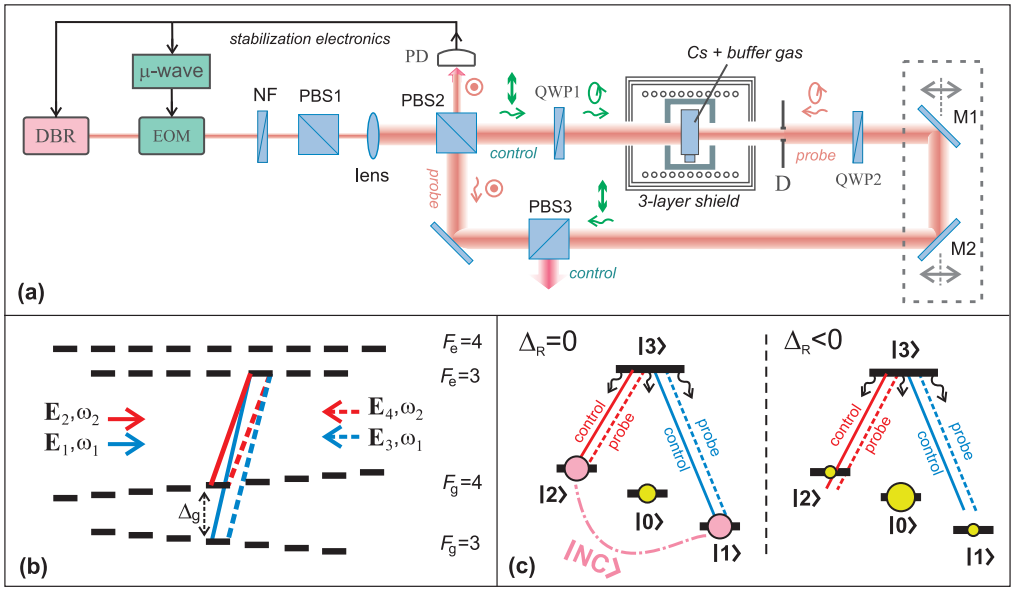

Fig. 1. (a) Experimental setup. DBR: DBR laser, EOM: intensity electro-optic modulator, μ-wave: microwave frequency synthesizer, PBS: polarizing beam splitter, PD: photodetector, QWP: quarter-wave plate, M1 and M2: two mirrors on a translation stage, D: iris diaphragm. (b) Simplified scheme of the Cs D_1 line energy levels involved in the EIA experiment. Atoms are assumed to be at rest. The vertical lines denote σ^+ light-induced transitions which are in two-photon resonance with the atoms. Blue and red lines stand for ω_1 and ω_2 angular optical frequencies, respectively. The other transitions are not in resonance and are not shown. Δ_g stands for the microwave frequency of the ground-state hyperfine splitting. A static magnetic field is applied parallel to the wave vectors to frequency-split the ground-state levels. The splitting of the excited-state levels is not relevant in our study. (c) Λ-scheme of atomic energy levels under the two-photon resonance (left) and not in the resonance (right). Circles reflect qualitatively the energy-level populations. The pink color is for the atoms in the CPT dark state, while the yellow color is for other atoms. Wavy arrows denote spontaneous decay.

(Ne:Ar = 20:2 Torr). The cell is heated by a thermochamber made of copper. A longitudinal static magnetic field of 450 mG is produced by a solenoid in order to eliminate the degeneracy of the cesium ground states and isolate the "0-0" two-photon clock transition. A three-layer μ-metal magnetic shield is used to prevent perturbations from the ambient magnetic field on the clock transition.

2.2. *Qualitative description*

The present EIA resonance detection scheme presents two key differences in comparison with the σ^+–σ^- scheme proposed in [17] for the detection of a dark resonance. The first point is that counterpropagating beams with equal circular polarizations are used. The second point is that the condition $I_p \ll I_c$, with I_p and I_c the intensities of the probe and control beams respectively, must be satisfied. The observation of bright resonances in the proposed scheme can be explained by a simplified Λ-model (Fig. 1(c)). This model, commonly used to study CPT and related effects [6], implies two ground-state levels $|1\rangle$ and $|2\rangle$, an excited-state level $|3\rangle$ and an additional level $|0\rangle$ (optionally). The latter level does not interact with the light field, accumulates the atoms owing to optical pumping [20] and acts as a Zeeman trap state.

The laser field is composed of counterpropagating light beams traveling along the z-axis and can be described as:

$$E(z,t) = E_1 e^{-i(\omega_1 t - k_1 z)} + E_2 e^{-i(\omega_2 t - k_2 z)} \\ + E_3 e^{-i(\omega_1 t + k_1 z + \phi_1)} + E_4 e^{-i(\omega_2 t + k_2 z + \phi_2)} + c.c., \quad (1)$$

where $E_{1,2,3,4}$ are real amplitudes of the waves, $\omega_{1,2}$ are angular optical frequencies, $k_{1,2}$ are absolute values of the wave vectors, and $\phi_{1,2}$ are the time-independent phases.

In the case where only the two-frequency control field $\mathbf{E}_1$+$\mathbf{E}_2$ is present in the cell and the two-photon resonance condition is satisfied (with Δ_R=ω_1−ω_2−Δ_g=0 the Raman frequency detuning, see Fig. 1(b,c)), a non-coupled (NC) coherent superposition of levels $|1\rangle$ and $|2\rangle$ is created [6]. This state does not interact with the resonant light field and is responsible in the control-field vapor-cell transmission for the creation of a dark resonance. To derive an explicit form of the NC state, consider the operator of light-atom interaction in the dipole and rotating wave approximations (i.e., the time phases $i\omega_{1,2}t$ are excluded):

$$\hat{V} = -\hat{\mathbf{d}}(\mathbf{E}_1 + \mathbf{E}_2) = -\hbar R_c \left(e^{ik_1 z} |3\rangle\langle 1| + e^{ik_2 z} |3\rangle\langle 2| \right), \quad (2)$$

where $\hat{\mathbf{d}}$ is operator of the atom dipole momentum, R_c=$dE_c/\hbar$ is the Rabi frequency of the control field (we assume amplitudes of two light components $\mathbf{E_1}$ and $\mathbf{E_2}$ to be equal) with d being the matrix element of the dipole momentum operator.

It can be easily shown that the following state in the non-coupled state for the operator $\hat{V}$ (also see [17, 55]):

$$|\mathrm{NC}_1\rangle = \left(|1\rangle - e^{ik_{12}z} |2\rangle \right) \Big/ \sqrt{2}, \quad (3)$$

with k_{12}=$k_1 - k_2$. This state is an eigenvector with a zero eigenvalue, i.e.

$$\hat{V}|\mathrm{NC}_1\rangle = 0\,. \quad (4)$$

On the other hand, if only the probe field crosses the cell, another non-coupled superposition state can be created:

$$|\mathrm{NC}_2\rangle = \left(|1\rangle - e^{-i(k_{12}z + \phi_{12})} |2\rangle \right) \Big/ \sqrt{2}, \quad (5)$$

with ϕ_{12}=ϕ_1−ϕ_2.

The key point is then to understand that $|\mathrm{NC}_1\rangle$ and $|\mathrm{NC}_2\rangle$ states can be similar or essentially different, depending on the product $\left|\langle \mathrm{NC}_1 | \mathrm{NC}_2 \rangle\right|$ such that:

$$\left|\langle \mathrm{NC}_1 | \mathrm{NC}_2 \rangle\right| = \sin\left(k_{12}z + \phi_{12}/2\right). \quad (6)$$

If the product $\left|\langle \mathrm{NC}_1 | \mathrm{NC}_2 \rangle\right|$ is unity, both non-coupled states are similar and are dark for the probe field. This situation leads to the observation of a dark resonance. At the opposite, if $|\mathrm{NC}_1\rangle$ and $|\mathrm{NC}_2\rangle$ are orthogonal, the probe beam may experience strong absorption [55, 56]. In a long enough cell, regions with strong probe-field absorption (bright regions) alternate then with regions of low probe-field absorption (dark regions). From (6), the period of these oscillations is given by:

$$\Delta z = \pi \big/ |k_{12}|\,, \quad (7)$$

with $\Delta z \approx 1.6$ cm for Cs atom. The signature of these spatial oscillations is then expected to be better revealed in short-length cells (L<Δz) since a short cell could be placed in a region where the probe-field absorption is maximum. At the same time, the cell length should not be too small to keep the benefit from the spatial oscillation effect. The optimal cell length can be estimated to

be about $\Delta z/4$. For Cs atom, this yields a length of about 4 mm, comparable to the length of the cell (5 mm) used in our experiments.

In a short cell, the absorption of the medium remains about constant, so that the oscillations (6) over the cell length can be neglected, i.e. $z \equiv z_c$ can be considered in (6) with z_c being the position of the cell. Analogously, the optimization of the probe-wave absorption can be achieved by adjusting the phase ϕ_{12}. In our experiments, this adjustment is done by shifting the mirrors M1 and M2 shown in Fig. 1(a). Since shifting the mirrors by Δz is identical to shifting the cell by $2\Delta z$, bright resonances alternate with dark resonances with a period $\Delta z/2 \approx 0.8$ cm during the mirrors scan.

To obtain an EIA resonance with the highest contrast, the probe-field absorption must be high at $\Delta_R=0$ and low at $\Delta_R \gg \Delta_{res}$, where Δ_{res} is the full-width at half-maximum (FWHM) of the resonance. At $\Delta_R=0$, the high absorption occurs when $|NC_1\rangle$ and $|NC_2\rangle$ are orthogonal. Figure 1(c) (right) shows that at $\Delta_R \gg \Delta_{res}$, a low probe field absorption can be achieved by pumping optically most of the atoms into the trap level $|0\rangle$. Indeed, if $\Delta_R \gg \Delta_{res}$, the non-coupled state $|NC_1\rangle$ is not created and the control field pumps atoms out of $|1\rangle$ and $|2\rangle$ levels.

In EIT or CPT resonances, the configuration $\sigma^+ - \sigma^-$ is often used in order to eliminate the trap states and to increase the contrast of the dark resonances [18]. At the opposite, Zeeman trap states can play a positive role in the case of bright EIA resonances by inducing a reduced absorption at $\Delta_R \gg \Delta_{res}$. However, since the probe-wave absorption is also high at $\Delta_R=0$ due to the creation of the $|NC_1\rangle$ state, the final contrast of the EIA resonance could be quite low. To circumvent this issue, counterpropagating beams with identical circular polarizations are used in the present work to let the trap states survive and to observe the EIA effect.

This analysis explains also the reason why the probe field should be much weaker than the control field. With two counterpropagating beams of equal intensities, any non-coupled state cannot be created due to the "competition" between orthogonal $|NC_1\rangle$ and $|NC_2\rangle$ states. In this case, most of the atoms are transferred to a trap level $|0\rangle$ by optical pumping, leading to a significant decrease of the probe-field absorption at the center of the resonance ($\Delta_R=0$).

2.3. EIA spectroscopy

Figure 2 shows some examples of EIA resonances observed in the probe wave transmission by sweeping the Raman frequency detuning Δ_R. In the first case, the resonance line, shown in green, is a typical EIA clock resonance. Obtained here with a control beam power P_c and probe beam power P_p of 40 and 4.5 μW respectively, the EIA resonance exhibits a FWHM of 850 Hz and a contrast of 2.5% with respect to the background light transmission. The second case is an illustration of the quasi-disappearance of the EIA resonance when required conditions are not satisfied. As mentioned previously, the sign of the subnatural-linewidth resonance (enhanced absorption or transparency) depends on the relative phase between both counterpropagating beams. In addition, the EIA resonance disappears when both probe and control beams have similar intensities. This situation is illustrated by the blue line on Fig. 2 where the resonance contrast is degraded to 0.1%. Note that the experiment is performed in a large optical density regime in which both the probe wave and the pump wave experience significant absorption in the cell (about 50%). Therefore, the intensity of both waves in the cell is not constant and the probe wave can be weaker than the control one in some regions of the cell, explaining the residual EIA dip in the center of the blue line profile. For illustration, let us consider a sketch shown in Fig. 3. When light wave intensities are equal at the cell entrance, only the central part of the cell is exposed to light waves of equal strengths (region "II"). In this region, there are no $|NC_1\rangle$ as well as $|NC_2\rangle$ states because of their "competition". At the same time, in the regions "I" and "III", the light wave intensities are different, leading to the EIA effect in the former case and to the EIT effect in the latter case. This basic treatment helps to explain the non-vanishing EIA resonance in Fig. 2 (blue curve) superimposed with a broad EIT background profile.

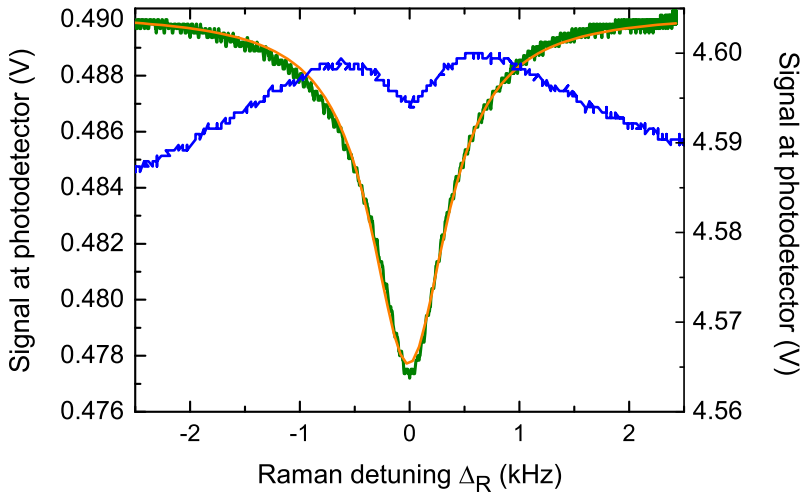

Fig. 2. Detection of EIA resonances. In the first case with light beams of different intensities (green steep dip, left "y" axis), the typical clock EIA resonance is observed. The resonance linewidth is 850 Hz and the resonance contrast is 2.5%. Experimental data are fitted by a Lorentzian function. The cell temperature is 60°C. The control and probe beam powers are 40 μW and 4.5 μW respectively. In the second case (blue line and right "y" axis), the EIA resonance is almost absent, having extremely low contrast of about 0.13%. This occurs when the beams have close powers: $P_c \approx P_p$=40 μW.

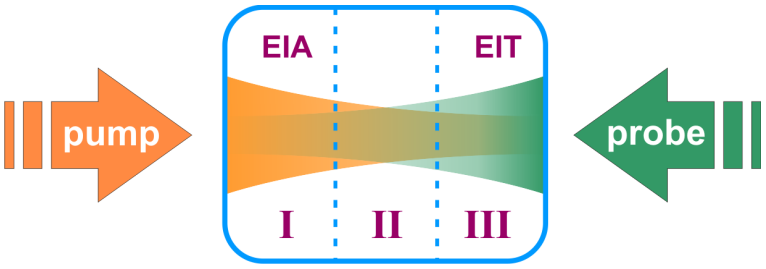

Fig. 3. Sketch of light field absorption in a vapor cell under the regime of equal intensities of counterpropagating waves. EIA and EIT denote the regions which contribute to the creation of subnatural-linewidth absorption and transparency resonances in the probe wave transmission signal (see blue curve in Fig. 2). The effect of spatial oscillations of the light field absorption within the cell is neglected since the cell is sufficiently short.

Figure 4 shows the evolution of the EIA resonance linewidth and height versus the control beam intensity I_c. Experimental linewidth data are correctly fitted by a linear function such that FWHM [kHz] = 3.2 I_c + 0.58, with I_c in mW/cm^2. This linear behavior is typical for subnatural-linewidth resonances in buffer-gas-filled vapor cells [9, 10]. In our experiment, the main contribution to the zero-intensity linewidth is the time-of-flight relaxation process, due to the finite light beam size and then the limited atom-field interaction time. Using expressions reported in [57], this contribution is calculated to give a zero-intensity linewidth of 450 Hz, in correct agreement with the experimental result of 580 Hz.

The height of the EIA resonance increases rapidly at small control wave intensities, while at higher intensities this growth is slower. The latter can be interpreted as the saturation of the differential probe-wave absorption coefficient $\Delta\alpha(I_c)=\alpha_0-\alpha_1$ with $\alpha_{0,1}$ the absorption coefficients

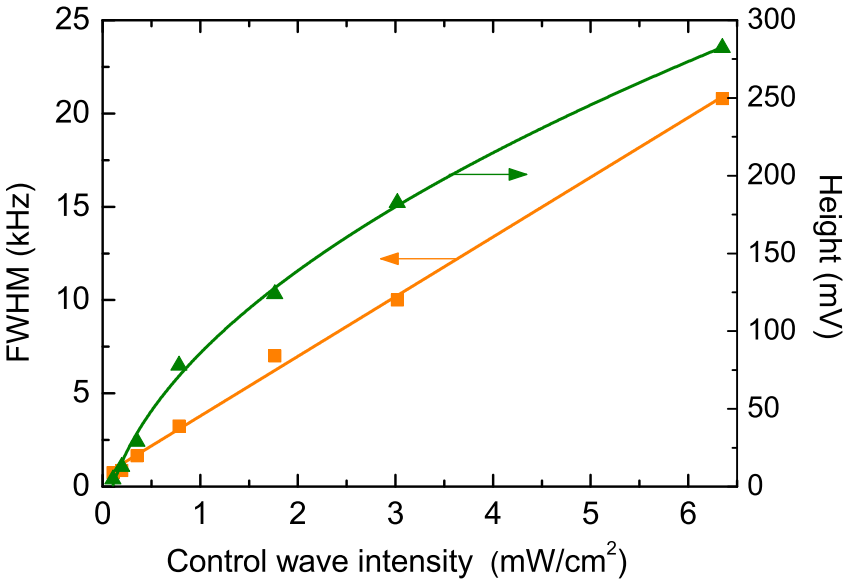

Fig. 4. FWHM (squares) and signal (triangles) of the EIA resonance versus the control wave intensity. Experimental linewidth data are fitted by a linear function, yielding a linewidth extrapolated at null laser intensity of 580 Hz. The cell temperature is 60°C. The probe beam power is about 1/9 of the control beam power.

in the center of the EIA resonance (0) and out of it (1). From linewidth and signal data, we were able to find that the signal/linewidth ratio was maximized for quite low control laser intensities, typically lower than 0.5 mW/cm^2.

3. EIA-clock short-term stability

Figure 5 reports the preliminary Allan deviation of the EIA-based atomic clock. This measurement was performed for laser powers (P_c=40 μW, P_p=4.5 μW) and cell temperature (60°C) conditions optimizing the signal/linewidth ratio. In this experiment, the laser frequency is simply stabilized onto the bottom of the homogeneously-broadened absorption profile using a standard synchronous modulation-demodulation technique. No sub-Doppler spectroscopy technique for enhanced laser frequency stabilization is used. The microwave frequency is stabilized using the Pound-Drever-Hall (PDH) technique. Modulating the LO frequency, each optical sideband is accompanied by two additional first-order radiofrequency (RF) sidebands, each separated from the optical sideband by the LO modulation frequency (9.36 kHz in our case). In the case where the LO modulation frequency is higher than the linewidth of the EIA resonance, three separate EIA resonances are observed at the output of the detection photodiode. Phase-sensitive demodulation is then produced and the quadrature signal is used for stabilization of the microwave frequency. The phase of the modulation signal is here a crucial parameter and was optimized by maximizing the slope of the output error signal. Compared to conventional synchronous modulation-demodulation approaches, the main advantage of the PDH technique is to modulate the LO frequency at higher frequency, yielding a relevant reduction of the detection noise level. The LO modulation frequency (9.36 kHz) was chosen to avoid any spurious intermodulation effects with other frequency components existing in our electronics (50 Hz and harmonics for example) and any cross-talk issues with the laser frequency stabilization loop. The EIA resonance used for clock operation is shown in Fig. 2 (green line). The frequency stability of the stabilized LO is measured

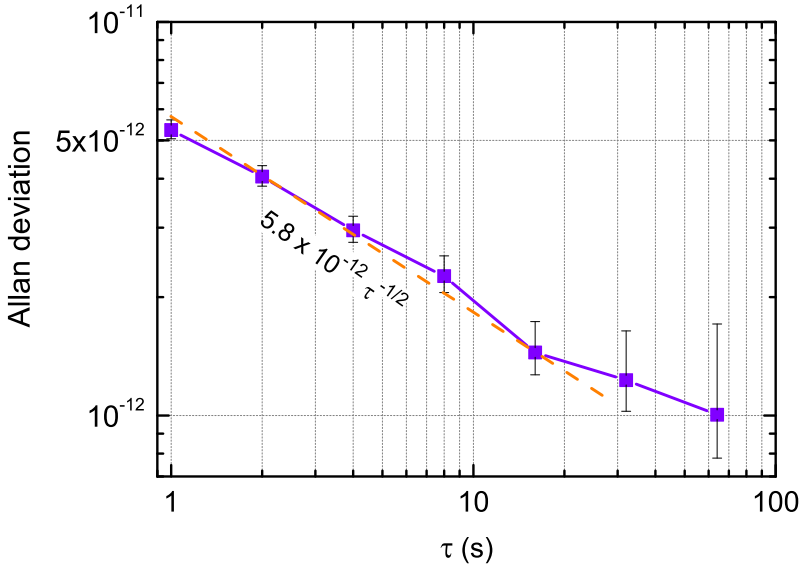

Fig. 5. Short-term fractional frequency stability of the EIA-based atomic clock.

by comparison with a passive hydrogen maser reference standard.

The short-term frequency stability of an atomic clock can be well-approximated by σ_y (1 s) $\approx$ (FWHM / ν_0) $\times$ (1/SNR), with ν_0 the clock frequency and SNR the signal-to-noise ratio of the resonance in a 1 Hz bandwidth. In our experimental setup, measurements of the total detection noise (7.6×10^{-6} V/$\sqrt{\text{Hz}}$ at f_m=9.36 kHz where f_m is the LO modulation frequency) at the output of the photodiode led to a measured SNR of about 20330, yielding an expected short-term stability of 4.6×10^{-12} at 1 s. This expected value is in correct agreement with the measured stability value shown on Fig. 5, found to be 5.8×10^{-12} $\tau^{-1/2}$ until 20 s and at the level of 10^{-12} at 60 s averaging time.

Table 1 shows main contributions to the EIA-clock short-term stability budget. The main contribution to the EIA clock short-term stability is the total laser noise (laser FM noise through

Table 1. Contributions to the EIA clock short-term frequency stability budget. Expressions similar to those reported in [27] combined with detection noise measurements were used for these estimations. FM and AM stand for laser frequency and amplitude noise, respectively.

Noise source	Contribution to σ_y (1s)
Photon shot noise	1.5×10^{-12}
Detector noise	1.5×10^{-12}
LO phase noise	$< 1 \times 10^{-12}$
Total laser noise (FM and AM)	4.6×10^{-12}
$\sigma_y(1s) = \sqrt{\sum \sigma_y^2}$	4.6×10^{-12}

the FM-AM conversion process in the cell and laser AM noise). Note that the laser frequency noise contribution could be reduced by stabilizing the laser frequency onto an external reference cell using a Doppler-free spectroscopy technique. The measured short-term stability is 3.5 times higher than the calculated photon shot noise. On slightly higher time scales, we suspect that the clock frequency stability might be limited by the fluctuations of the optical beam path length. Indeed, a relevant sensitivity of the clock frequency to the mirrors translation at the level of 10 mHz/μm, i.e. $1.1 \times 10^{-12}/\mu$m in fractional value, has been measured. To date, no optical path length stabilization is implemented in our setup and many optical elements could experience acoustic and thermal fluctuations. We think that fractional length fluctuations of the optical path could be reduced at the level of 10^{-9} in a properly-designed low-vibration and reduced-size system with high-precision temperature control at the mK level. Such a length stability level would reject this contribution on the clock frequency stability below the 10^{-15} level. For improved length stabilization, interferometer-based techniques inspired from the domains of optical fiber links [58] or ultra-stable lasers [59] might be envisioned but at the expense of a relevant increase of the clock architecture complexity.

The preliminary short-term frequency stability of the EIA-clock remains to date about a factor of 10–30 lower than those of best CPT-based vapor-cell atomic clocks [27,29]. Compared to these CPT clocks, an advantage of the present EIA scheme is to benefit from the use of short-length cells. The present EIA-clock uses a 5-mm long cell whereas CPT clocks described in [27,29] are based on 5-cm long cells. The current short-term stability performances of the EIA-clock remain encouraging since they compare favorably with those of a N-resonance atomic clock based on a 7.5-cm long vapor cell [31] or other CPT-based clock prototypes [18, 60, 61]. For further progress, the laser FM noise contribution to the short-term stability budget could be reduced by stabilizing the laser using sub-Doppler spectroscopy techniques [56, 62]. In addition, we suppose that the EIA clock should benefit from the use of Ramsey-based interrogation protocols, both for reduction of the photon shot noise contribution since higher laser powers might be used and mitigation of light shift issues [28, 29, 63–65].

4. Conclusions

We have proposed a dual-frequency optical field configuration scheme that allows the detection of narrow-linewidth EIA resonances in a buffer-gas filled alkali vapor cell. At the contrary of previously-reported EIA schemes, the EIA resonance detection is achieved in the present setup by tuning the laser frequency difference between both optical fields at fixed static magnetic field. Microwave frequency stabilization onto a sub-kHz linewidth EIA resonance was performed in order to achieve an atomic clock. The EIA atomic clock exhibits a preliminary Allan deviation of $5.8\times10^{-12}\tau^{-1/2}$ up to 20 s, in correct agreement with the signal-to-noise ratio and linewidth of the detected resonance. Exploration paths to be studied in the future were suggested to optimize further the EIA clock fractional frequency stability performances.

Funding

Russian Science Foundation (RSF) (17-72-20089). Région Bourgogne Franche-Comté, Agence Nationale de la Recherche (Labex FIRST-TF, Grant 10-LABX-0048, Oscilator-IMP Grant 11-EQPX-0033).

Acknowledgments

We thank Nikolay Kvashnin, Vadim Vasiliev and Alexey Lugovoy (Institute of Laser Physics SB RAS) for their help with electronics and software. R. Boudot thanks Jacques Millo, Enrico Rubiola and Vincent Giordano (FEMTO-ST) for fruitful discussions.

References

1. S. Stenholm, *Foundations of laser spectroscopy* (Wiley Verlag, 1984).
2. A. Aspect, E. Arimondo, R. Kaizer, N. Vansteenkiste, and C. Cohen-Tannoudji, "Laser cooling below the one-photon recoil energy by velocity-selective coherent population trapping: theoretical analysis," J. Opt. Soc. Am. B **6**(11), 2112–2124 (1989).
3. J. Kitching, "Chip-scale atomic devices," Appl. Phys. Rev. **5**, 031302 (2018).
4. M. Fleischhauer, A. Imamoglu, and J. P. Marangos, "Electromagnetically induced transparency: Optics in coherent media," Rev. Mod. Phys. **77**(2), 633–674 (2005).
5. A. Alzetta, A. Gozzini, L. Moi, and G. Orriols, "An experimental method for the observation of r.f. transitions and laser beat resonances in oriented Na vapour," Nuovo Cimento B **36**(1), 5–20 (1976).
6. E. Arimondo, "Coherent population trapping in laser spectroscopy," Prog. Opt. **35**, 257–354 (1996).
7. A. M. Akulshin, S. Barreiro, and A. Lezama, "Electromagnetically induced absorption and transparency due to resonant two-field excitation of quasidegenerate levels in Rb vapor," Phys. Rev. A **57**(4), 2996–3002 (1998).
8. A. S. Zibrov, M. D. Lukin, L. Hollberg, D. E. Nikonov, M. O. Scully, H. G. Robinson, and V. L. Velichansky, "Experimental demonstration of enhanced index of refraction via quantum coherence in Rb," Phys. Rev. Lett. **76**(21), 3935–3938 (1996).
9. J. Vanier, A. Godone, and F. Levi, "Coherent population trapping in cesium: Dark lines and coherent microwave emission," Phys. Rev. A **58**(3), 2345-2358 (1998).
10. R. Wynands and A. Nagel, "Precision spectroscopy with coherent dark states," Appl. Phys. B **68**, 1–25 (1999).
11. M. A. Bouchiat and J. Brossel, "Relaxation of optically pumped Rb atoms on paraffin-coated walls," Phys. Rev. **147**(1), 41–54 (1966).
12. M. Klein, I. Novikova, D. F. Phillips, and R. L. Walsworth, "Slow light in paraffin-coated Rb vapour cells," J. Mod. Opt. **53**(16-17), 2583–2591 (2006).
13. M. V. Balabas, T. Karaulanov, M. P. Ledbetter, and D. Budker, "Polarized alkali-metal vapor with minute-long transverse spin-relaxation time," Phys. Rev. Lett. **105**(7), 070801 (2010).
14. F. X. Esnault, E. Blanshan, E. N. Ivanov, R. E. Scholten, J. Kitching, and E. A. Donley, "Cold-atom double-Λ coherent population trapping clock," Phys. Rev. A **88**(4), 042120 (2013).
15. N. Cyr, M. Têtu, and M. Breton, "All-optical microwave frequency standard: a proposal," IEEE Trans. Instrum. Meas. **42**(2), 640–649 (1993).
16. M. Stähler, R. Wynands, S. Knappe, J. Kitching, L. Hollberg, A. V. Taichenachev, and V. I. Yudin, "Coherent population trapping resonances in thermal ^{85}Rb vapor: D_1 versus D_2 line excitation," Opt. Lett. **27**(16), 1472–1474 (2002).
17. A. V. Taichenachev, V. I. Yudin, V. L. Velichansky, S. V. Kargapoltsev, R. Wynands, J. Kitching, and L. Hollberg, "High-contrast dark resonances on the D_1 line of alkali metals in the field of counterpropagating waves," JETP Lett. **80**(4), 236–240 (2004).
18. X. Liu, V. I. Yudin, A. V. Taichenachev, J. Kitching, and E. A. Donley, "High contrast dark resonances in a cold-atom clock probed with counterpropagating circularly polarized beams," Appl. Phys. Lett. **111**(22), 224102 (2017).
19. A. V. Taichenachev, V. I. Yudin, V. L. Velichansky, and S. A. Zibrov, "On the unique possibility to increase significantly the contrast of dark resonances on D_1 line of ^{87}Rb," JETP Lett. **82**(7), 398–403 (2005).
20. K. Watabe, T. Ikegami, A. Takamizawa, S. Yanagimachi, S. Ohshima, and S. Knappe, "High-contrast dark resonances with linearly polarized light on the D_1 line of alkali atoms with large nuclear spin," Appl. Opt. **48**(6), 1098–1103 (2009).
21. T. Zanon, S. Guérandel, E. de Clercq, D. Holleville, N. Dimarcq, and A. Clairon, "High contrast Ramsey fringes with coherent-population-trapping pulses in a double Lambda atomic system," Phys. Rev. Lett. **94**(19), 193002 (2005).
22. Y.-Y. Jau, E. Miron, A. B. Post, N. N. Kuzma, and W. Happer, "Push-pull optical pumping of pure superposition states," Phys. Rev. Lett. **93**(16), 160802 (2004).
23. X. Liu, J.-M. Mérolla, S. Guérandel, C. Gorecki, E. de Clercq, and R. Boudot, "Coherent-population-trapping resonances in buffer-gas-filled Cs-vapor cells with push-pull optical pumping," Phys. Rev. A **87**(1), 013416 (2013).
24. P. Yun, J.-M. Danet, D. Holleville, E. de Clercq, and S. Guérandel, "Constructive polarization modulation for coherent population trapping clock," Appl. Phys. Lett. **105**(23), 231106 (2014).
25. T. Zanon-Willette, R. Lefevre, R. Metzdorff, N. Sillitoe, S. Almonacil, M. Minissale, E. de Clercq, A. V. Taichenachev, V. I. Yudin, and E. Arimondo, "Composite laser-pulses spectroscopy for high-accuracy optical clocks: a review of recent progress and perspectives," Rep. Prog. Phys. **81**(9), 094401 (2018).
26. M. Abdel Hafiz, G. Coget, P. Yun, S. Guérandel, E. de Clercq and R. Boudot "A high-performance Raman-Ramsey Cs vapor cell atomic clock," J. Appl. Phys. **121**, 104903 (2017).
27. P. Yun, F. Tricot, C. E. Calosso, S. Micalizio, B. Francois, R. Boudot, S. Guérandel and E. de Clercq "High-performance coherent population trapping clock with polarization modulation," Phys. Rev. Appl. **7**, 014018 (2017).
28. M. Abdel Hafiz, G. Coget, M. Petersen, C. Rocher, S. Guérandel, T. Zanon-Willette, E. de Clercq and R. Boudot, "Toward a high-stability coherent population trapping Cs vapor-cell atomic clock using autobalanced Ramsey spectroscopy," Phys. Rev. Appl. **9**, 064002 (2018).
29. M. Abdel Hafiz, G. Coget, M. Petersen, C. Calosso, S. Guérandel, E. de Clercq, and R. Boudot, "Symmetric autobalanced Ramsey interrogation for high-performance coherent-population-trapping vapor-cell atomic clock," Appl. Phys. Lett. **112**(24), 244102 (2018).

30. M. A. Guidry, E. Kuchina, I. Novikova, and E. E. Mikhailov, "Characterization of frequency stability in electromagnetically induced transparency-based atomic clocks using a differential detection scheme," J. Opt. Soc. Am. B **34**(10), 2244-2249 (2017).
31. I. Novikova, D. F. Phillips, A. S. Zibrov, R. L. Walsworth, A. V. Taichenachev, and V. I. Yudin, "Cancellation of light shifts in an N-resonance clock," Opt. Lett. **31**(5), 622–624 (2006).
32. A. V. Taichenachev, A. M. Tumaikin, and V. I. Yudin, "On the spontaneous-coherence-transfer-induced sign change of a sub-natural-width nonlinear resonance," JETP Lett. **69**(11), 819–824 (1999).
33. C. Goren, A. D. Wilson-Gordon, M. Rosenbluh, and H. Friedmann, "Electromagnetically induced absorption due to transfer of coherence and to transfer of population," Phys. Rev. A **67**(3), 033807 (2003).
34. D. B. Lazebnyi, D. V. Brazhnikov, A. V. Taichenachev, M. Yu. Basalaev, and V. I. Yudin, "Electromagnetically induced absorption and electromagnetically induced transparency for optical transitions $F_g \rightarrow F_e$ in the field of elliptically polarized waves," J. Exp. Theor. Phys. **121**(6), 934–949 (2015).
35. A. Sargsyan, D. Sarkisyan, Y. Pashayan-Leroy, C. Leroy, S. Cartaleva, A. D. Wilson-Gordon, and M. Auzinsh, "Electromagnetically induced transparency resonances inverted in magnetic field," J. Exp. Theor. Phys. **121**(6), 966–975 (2015).
36. Y. Dancheva, G. Alzetta, S. Cartaleva, M. Taslakov, and Ch. Andreeva, Opt. Commun. **178**(1-3), 103–110 (2000).
37. F. Renzoni, S. Cartaleva, G. Alzetta, and E. Arimondo, "Enhanced absorption Hanle effect in the configuration of crossed laser beam and magnetic field," Phys. Rev. A **63**(6), 065401 (2001).
38. C. Affolderbach, S. Knappe, R. Wynands, A. V. Taĭchenachev, and V. I. Yudin, "Electromagnetically induced transparency and absorption in a standing wave," Phys. Rev. A **65**(4), 043810 (2002).
39. C. Andreeva, S. Cartaleva, Y. Dancheva, V. Biancalana, A. Burchianti, C. Marinelli, E. Mariotti, L. Moi, and K. Nasyrov, "Coherent spectroscopy of degenerate two-level systems in Cs," Phys. Rev. A **66**(1), 012502 (2002).
40. A.V. Papoyan, M. Auzinsh, and K. Bergmann, "Nonlinear Hanle effect in Cs vapor under strong laser excitation," Eur. Phys. J. D **21**(1), 63–71 (2002).
41. E. E. Mikhailov, I. Novikova, Y. V. Rostovtsev, and G. R. Welch, "Buffer-gas-induced absorption resonances in Rb vapor," Phys. Rev. A **70**(3), 033806 (2004).
42. J. Fuchs, G. J. Duffy, W. J. Rowlands, A. Lezama, P. Hannaford, and A. M. Akulshin, "Electromagnetically induced transparency and absorption due to optical and ground-state coherences in ^{6}Li," J. Phys. B: At. Mol. Opt. Phys. **40**(6), 1117–1129 (2007).
43. A. A. Zhukov, S. A. Zibrov, G. V. Romanov, Y. O. Dudin, V. V. Vassiliev, V. L. Velichansky, and V. P. Yakovlev, "Electromagnetically induced absorption in a bichromatic laser field," Phys. Rev. A **80**(3), 033830 (2009).
44. A. Sargsyan, A. Papoyan, A. Sarkisyan, Yu. Malakyan, G. Grigoryan, D. Sarkisyan, Y. Pashayan-Leroy, C. Leroy, "Narrow and contrast resonance of increased absorption in Λ-system observed in Rb cell with buffer gas," Armenian J. Phys. **2**(2), 84–94 (2009).
45. H.-J. Kim and H. S. Moon, "Electromagnetically induced absorption with sub-kHz spectral width in a paraffin-coated Rb vapor cell," Opt. Express **19**(1), 168–174 (2011).
46. Z. D. Grujić, M. M. Lekić, M. Radonjić, D. Arsenović, and B. M. Jelenković, "Ramsey effects in coherent resonances at closed transition F_g=2→F_e=3 of ^{87}Rb," J. Phys. B: At. Mol. Opt. Phys. **45**(24), 245502 (2012).
47. Y. Ma, J. Deng, Z. Hu, H. He, and Y. Wang, "Microwave excited optical transparency enhancement resonances in Hanle-EIT configuration," Chin. Opt. Lett. **11**(2) 022701 (2013).
48. D. V. Brazhnikov, A. V. Taichenachev, A. M. Tumaikin, and V. I. Yudin, "Electromagnetically-induced-absorption resonance with high contrast and narrow width in the Hanle configuration," Laser Phys. Lett. **11**(12), 125702 (2014).
49. D. J. Whiting, E. Bimbard, J. Keaveney, M. A. Zentile, C. S. Adams, and I. G. Hughes, "Electromagnetically induced absorption in a nondegenerate three-level ladder system," Opt. Lett. **40**(18), 4289–4292 (2015).
50. S. Gozzini, A. Fioretti, A. Lucchesini, L. Marmugi, C. Marinelli, S. Tsvetkov, S. Gateva, and S. Cartaleva, "Tunable and polarization-controlled high-contrast bright and dark coherent resonances in potassium," Opt. Lett. **42**(15), 2930–2933 (2017).
51. H. Ravi, M. Bhattarai, V. Bharti, and V. Natarajan, "Polarization-dependent tuning of the Hanle effect in the ground state of Cs," Europhys. Lett. **117**(6), 63002 (2017).
52. D. V. Brazhnikov, S. M. Ignatovich, V. I. Vishnyakov, M. N. Skvortsov, Ch. Andreeva, V. M. Entin, and I. I. Ryabtsev, "High-quality electromagnetically-induced absorption resonances in a buffer-gas-filled vapour cell," Laser Phys. Lett. **15**(2), 025701 (2018).
53. M. Bhattarai, V. Bharti, and V. Natarajan, "Tuning of the Hanle effect from EIT to EIA using spatially separated probe and control beams," Sci. Rep. **8**, 7525 (2018).
54. D. V. Brazhnikov, S. M. Ignatovich, A. S. Novokreshchenov, and M. N. Skvortsov, "Ultrahigh-quality electromagnetically induced absorption resonances in a cesium vapor cell," J. Phys. B: At. Mol. Opt. Phys. **52**, 215002 (2019).
55. M. Abdel Hafiz, D. V. Brazhnikov, G. Coget, A. V. Taichenachev, V. I. Yudin, E. de Clercq, and R. Boudot, "High-contrast sub-Doppler absorption spikes in a hot atomic vapor cell exposed to a dual-frequency laser field," New J. Phys. **19**, 073028 (2017).
56. D. V. Brazhnikov, M. Petersen, G. Coget, N. Passilly, V. Maurice, C. Gorecki, and R. Boudot, "Dual-frequency sub-Doppler spectroscopy: Extended theoretical model and microcell-based experiments," Phys. Rev. A **99**(6), 062508 (2019).

57. J. Vanier and C. Audoin, *The Quantum Physics of Atomic Frequency Standards* (Adam Hilger, Bristol, England, 1989).
58. M. Musha, Y. Sato, K. Nakagawa, K. Ueda, A. Ueda, M. Ishiguro, "Robust and precise length stabilization of a 25-km long optical fiber using an optical interferometric method with a digital phase-frequency discriminator," Opt. Lett. **82**(4), 555–559 (2006).
59. F. Kefelian, H. Jiang, P. Lemonde and G. Santarelli, "Ultralow-frequency-noise stabilization of a laser by locking to an optical fiber-delay line," Opt. Lett. **34**(7), 914–916 (2009).
60. E. E. Mikhailov, T. Horrom, N. Belcher, and I. Novikova, "Performance of a prototype atomic clock based on $lin||lin$ coherent population trapping resonances in Rb atomic vapor," J. Opt. Soc. Am. B **27**(3), 417–422 (2010).
61. Z. Warren, M. S. Shahriar, R. Tripathi, and G. S. Pati, "Experimental and theoretical comparison of different optical excitation schemes for a compact coherent population trapping Rb vapor clock," Metrologia **54**(4), 418–431 (2017).
62. M. Abdel Hafiz, G. Coget, E. de Clercq and R. Boudot, "Doppler-free spectroscopy on the Cs D_1 line with a dual-frequency laser," Opt. Lett. **41**(13), 2982–2985 (2016).
63. M. Shuker, J. W. Pollock, R. Boudot, V. I. Yudin, A. V. Taichenachev, J. Kitching and E. A. Donley, "Ramsey spectroscopy with displaced frequency jumps," Phys. Rev. Lett. **122**, 113601 (2019).
64. M. Shuker, J. W. Pollock, R. Boudot, V. I. Yudin, A. V. Taichenachev, J. Kitching and E. A. Donley, "Reduction of light shifts in Ramsey spectroscopy with a combined error signal," Appl. Phys. Lett. **114**, 141106 (2019).
65. L. Lenci, L. Marmugi, F. Renzoni, S. Gozzini, A. Lucchesini and A. Fioretti, "Time-domain Ramsey-narrowed sub-kHz electromagnetically induced absorption in atomic potassium," J. Phys. B: At. Mol. Opt. Phys. **52**(8), 085002 (2019).